Dalton Transactions

Accepted Manuscript

ROYAL SOCIETY OF CHEMISTRY

www.rsc.org/dalton

Dalton Transactions

RSCPublishing

ARTICLE

Elucidating the mechanism responsible for anomalous thermal expansion in a Metal-Organic Framework

Cite this: DOI: 10.1039/x0xx00000x

Dewald P. van Heerden,[a] Catharine Esterhuysen[a]* and Leonard J. Barbour[a]*

Received ooth January 2015,
Accepted ooth January 2015

DOI: 10.1039/x0xx00000x

www.rsc.org/dalton

The previously reported anisotropic thermal expansion of a three-dimensional metal-organic framework (MOF) is examined by means of theoretical calculations. Inspection of the 100, 190, 280 and 370 K single crystal X-ray diffraction (SCD) structures indicated a concerted change in the coordination sphere of the zinc centre leading to elongation of the coordination helix in the crystallographic *c* direction (the Zn-O(H)-Zn angle expands), while the largely unaltered ligands (the Zn···L···Zn distance remains constant) are pulled closer together in the *ab* plane. This study develops and evaluates a mechanistic model at the DFT level of theory that reproduces the convergent expansion of the coordination helix of the material. The linear increase in energy calculated for extension of a model consisting of six zinc centres and truncated ligands compares favourably with results obtained from a periodic DFT evaluation of the SCD structures. It was also found that the anisotropic thermal expansion trend could be reproduced qualitatively by Molecular Dynamics (MD) simulations in the NPT ensemble.

Introduction

Most solids expand in all three dimensions with increasing temperature; that is, they undergo positive thermal expansion (PTE).[1] Each atom *i* vibrates about its mean position and, as the amplitude of vibration increase with increasing temperature, the anharmonic nature of interatomic potential wells causes distances between these mean positions to increase.[2] The thermal expansion of a material is its elastic response to the total thermal stress and this manifests as a change in volume at the macroscopic level.[3] The linear and volumetric coefficients of thermal expansion are defined as $\alpha = (\partial L/\partial T)_P/L$ and $\beta = (\partial V/\partial T)_P/V$, respectively, for an isobaric response in length L or volume V to an infinitesimal change in temperature T.[1] Isotropic solids (i.e. with cubic symmetry) have $\beta = 3\alpha$, but the situation is more complicated in the case of anisotropic solids where the linear expansion in the three orthogonal directions can be of different magnitudes and/or signs.[3]

Mechanisms other than vibrational modes are responsible for giant ($|\alpha| \geq 25 \times 10^{-6}$ K^{-1})[4] and colossal ($|\alpha| \geq 100 \times 10^{-6}$ K^{-1})[5] thermal expansion, with the supramolecular structure of a solid potentially being the determining factor responsible for its thermal behaviour.[3,4] The majority of structures known to exhibit negative thermal expansion (NTE) feature the M-O-M linkage.[3] To exhibit NTE, vibration modes transverse to the linkage must outweigh those occurring along it, resulting in a decrease of the effective M···M distance – the so-called "guitar string" effect.[6]

Isotropic NTE has been identified in the intensely studied MOF-5[7] ([Zn_4O(1,4-benzenedicarboxylate)$_3$], cubic crystal system, $Fm\bar{3}m$, a = 25.6690(3) Å).[8] This three-dimensional framework is composed of aromatic rings linking tetranuclear $Zn_4O(COO)_6$ clusters, wherein each zinc atom is bonded to three carboxylate oxygen atoms and a central oxygen dianion in a distorted tedrahedral fashion. Dubbeldam *et al.* successfully reproduced the observed NTE behaviour through MD simulations on one unit cell of MOF-5 in the NPT ensemble.[9] Subsequent MD simulations carried out by Han *et al.*[10] confirmed the findings of Dubbeldam *et al.* and found negligible changes in covalent bond lengths, while the average Zn-O coordination bond length increases by only Ψ0.010 Å as temperature is increased from 10 to 600 K. In line with the simulation results, an analysis of atomic displacement parameters from variable temperature SCD data led Lock *et al.* to conclude that the rigid Zn_4O clusters and aromatic linkers are connected through flexible carboxylate groups, allowing the aromatic rings to vibrate orthogonally, effectively reducing the mean distance between metal clusters and thus resulting in the NTE of MOF-5.[11]

[a] Department of Chemistry and Polymer Science, Stellenbosch University, South Africa. E-mail: ljb@sun.ac.za, ce@sun.ac.za

† Electronic Supplementary Information (ESI) available: derivation of equations involving mechanistic model, MD and DFT computational details, animation showing variation of mechanistic model. See DOI: 10.1039/x0xx00000x

Table 1 Summary of unit cell parameters and selected internal coordinates of full SCD structure determinations of **1** at different temperatures.[12]

CCDC deposition code	Temperature (K)	*a*, *b* axes (Å)	*c* axis (Å)	Zn···L···Zn (Å)	Zn-O(H)-Zn (°)	N-Zn-O_{carb} (°)
863858	100	26.5937(11)	5.1462(2)	12.1969(6)	126.7(1)	111.6(1)
863859	190	26.5112(9)	5.2351(1)	12.2056(6)	128.5(1)	112.0(1)
863860	280	26.4574(9)	5.2854(2)	12.1958(6)	129.6(2)	112.4(1)
863861	370	26.4366(9)	5.3287(2)	12.1926(7)	130.7(2)	113.5(3)

Similarly, it has been shown that the triply-interpenetrated framework $Ag_3[Co(CN)_6]$ displays colossal PTE in the basal plane of the trigonal unit cell with $\alpha_1 = 132 \times 10^{-6}$ K^{-1} and colossal NTE for the orthogonal *c* axis with $\alpha_3 = -130 \times 10^{-6}$ K^{-1}.[13] The framework, based on the crystal structure proposed by Pauling and Pauling,[14] consists of a network of Co-CN-Ag-NC-Co linkages wherein CoC_6 octahedra are connected through linear N-Ag-N bridges. A computational study by Calleja *et al.* highlighted the possible importance of an argentophilic interaction,[15] while a structural analysis by Conterio *et al.* revealed that the Co···Co chains remain linear, with little extension over the temperature range considered.[16] However, relatively large changes were identified in the C-Co-C valence angles. An anisotropic thermal expansion mechanism whereby rigid Co···Co linkages flex like a garden trellis therefore seems likely.[15] The similar magnitudes of the linear thermal expansion coefficients α_1 and α_3 corroborate such a mechanism whereby any expansion in the basal plane drives a contraction in the orthogonal *c* direction.

We have reported[12] a variable-temperature SCD analysis of a desolvated MOF (compound **1**: $[Zn(L)(OH)]_n$, L = 4-(1*H*-naphtho[2,3-*d*]imidazol-1-yl)benzoic acid under static vacuum, revealing colossal PTE along the *c* axis ($\alpha = 123 \times 10^{-6}$ K^{-1}) and biaxial NTE along the *a* and *b* axes ($\alpha = -21 \times 10^{-6}$ K^{-1}) – see Fig. 1b. The benzoate moiety is disordered over two positions of equal occupancy (see Fig. S2↔), with a full-occupancy oxygen atom coordinating to a Zn^{2+} cation, which is in a distorted tetrahedral coordination environment. The bridging hydroxide ion hydrogen bonds to the coordinating carboxylate oxygen atom to form a hydrogen bond network that interlaces the coordination helix along the crystallographic *c* axis, as depicted in Fig. 1c. Grobler *et al.* suggested that the mechanism responsible for the anisotropic thermal expansion is associated with the zinc-hydroxide-zinc coordination helix[12] since a flexible coordination geometry allows bond angles involving zinc atoms to deform to a greater extent than those involving the covalently bound atoms of the ligand.

In order to validate such a mechanism, we have developed a molecular model to reproduce the proposed convergent expansion of the coordination helix. Inspection of the previously determined 100, 190, 280 and 370 K SCD structures[12] indicated a concerted change in the coordination geometry of the zinc centre that results in elongation of the coordination helix in the *c* direction, while largely unaltered ligands (acting as rigid linkers) are pulled closer together in the *ab* plane. Table 1 shows the experimentally determined unit cell parameters, along with selected internal coordinates. The Zn···L···Zn distance remains essentially constant, decreasing by less than 0.02 Å in the temperature range considered, indicating that the coordination bond lengths between zinc centres and the rigid ligands undergo negligible changes. On the other hand, a systematic increase in the Zn-O(H)-Zn valence angle is symptomatic of stretching of the coordination helix with increasing temperature.

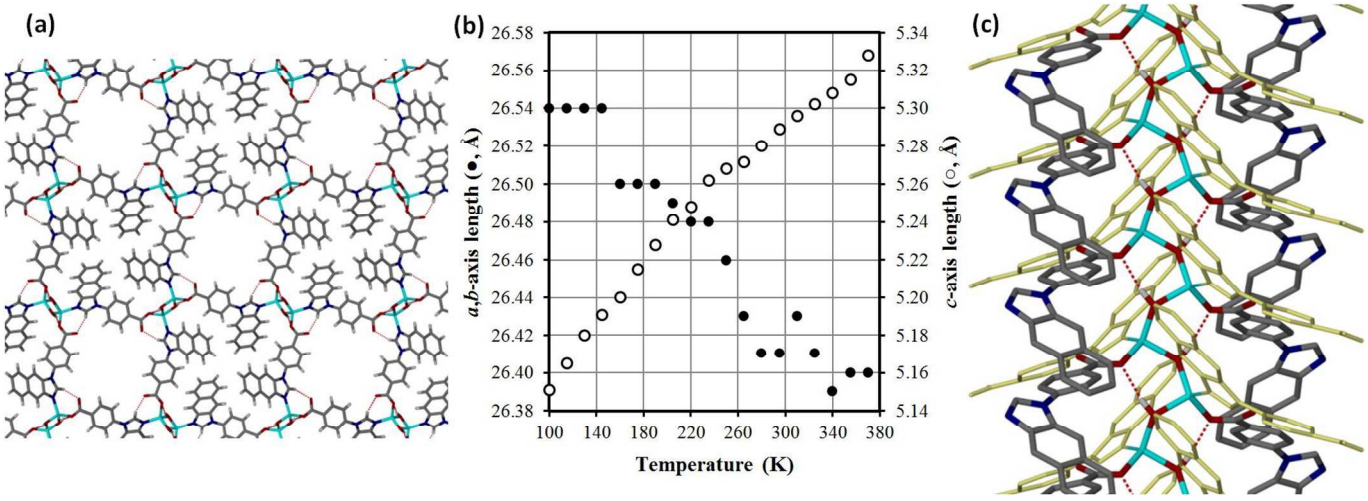

Fig. 1 (a) Packing of **1** viewed along [001] with only one position of the disordered benzoate moiety shown. (b) Graph of unit cell lengths determined by single crystal X-ray diffraction on the same crystal of **1** under static vacuum showing variation with temperature.[12] (c) Depiction of the hydrogen bond network (red dashed lines) interlacing the coordination helix viewed along [-110]. Here, only hydroxide hydrogen atoms are shown and ligands coordinating through the imidazole moiety are shown in yellow.

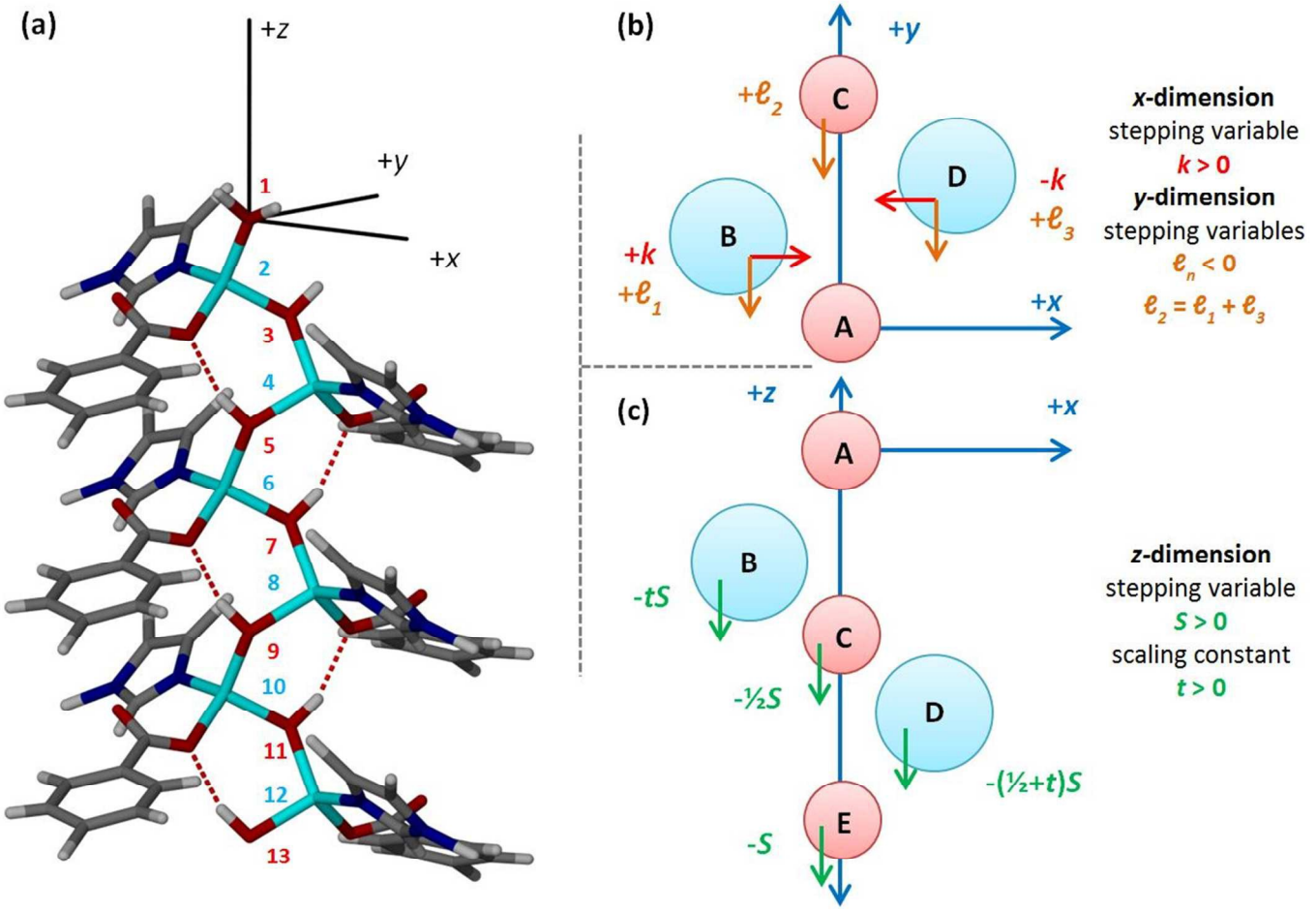

Fig. 2 (a) Molecular model consisting of six zinc centres and truncated ligands used to investigate anisotropic thermal expansion in **1**, with the labelling of the atoms in the coordination helix indicated in cyan for zinc atoms and red for the oxygen atoms of hydroxide groups. Hydrogen bonds between the hydroxide groups and coordinating benzoate oxygen atoms are shown as red dashed lines. Please note that one of the terminal hydroxide groups has been replaced with a coordinated water molecule to allow for charge neutrality; its oxygen atom (labelled 1) has been placed on the origin. One turn (or five atoms) of the coordination helix in the model is depicted on the right, with A, B, C, D and E corresponding to atoms O_1, Zn_2, O_3, Zn_4 and O_5, respectively. Oxygen atoms of hydroxide groups are shown as pink spheres and zinc atoms as larger cyan spheres. The variables controlling the convergent movement in the *xy* plane are shown in (b), while those of the extension in the *z* direction are shown in (c). Note that atoms A and E have the same *xy* coordinates and do not move in the *xy* plane during the simulation. The separation r_{AE} represents the effective *c* unit cell length, *c'*, which is increased by stepping the variable *S*.

Here we report a computational verification of the mechanism for the anisotropic thermal expansion of **1** proposed by Grobler *et al.*[18] with the aid of a simple mechanistic model. Energies from Density Functional Theory (DFT) evaluations of procured models are compared to results from periodic DFT calculations on SCD structures of **1**. Insight is also gained from variable temperature MD simulations on one unit cell of **1**.

Methods

Anisotropic thermal expansion mechanistic model

The geometry-optimized (*vide infra*) 100 K crystal structure of **1** was used to obtain a molecular representation, depicted in Fig. 2a, that consists of six zinc centres, with the hydroxide at one end of the coordination helix converted to a coordinating water molecule for charge neutrality. To reduce computational expense, the ligand was truncated to coordinating imidazole and benzoate moieties. The model was translated to position the coordinating water onto the origin, and rotated so that all O(H) *x* coordinates became zero ($x_A = x_C = 0$) and $x_B = -x_D$ (Fig. 2b). To specify their movement, atoms of the coordination helix (labelled as shown in Fig. 2a) are categorised into groups according to Table 2. Five atoms along the central helix describe a complete turn, with the fifth atom corresponding to the first atom at a separation of r_{AE}, which is initially equal to the 100 K *c* unit cell length. The convergent elongation of the coordination helix can be simulated by increasing this distance while simultaneously pulling all atoms closer to the *z*-axis. The translation variables of the *x*- and *y*-dimensions, specified by *k* and ℓ, respectively, are all defined in terms of a stepping variable in the *z*-dimension, designated *S*. The entire movement can therefore be controlled by a single parameter. For the purpose of brevity only key concepts are discussed here and the interested reader is referred to the ESI← for further details.

Table 2 Displacement of atoms (see text for details) labelled as shown in Fig. 2a, according to the parameters defined in Fig. 2b and c. Note from the last column that atoms of successive turns are translated by an additional *S* in the *z* direction, but by identical translations in the *xy* plane to corresponding atoms of previous turns.

Label	Group assignment	Δ*x*	Δ*y*	Δ*z*
1	A	0.0	0.0	0.0
2	B	$+k$	$+\ell_1$	$-tS$
3	C	0.0	$+\ell_2$	$-0.5S$
4	D	$-k$	$+\ell_3$	$-(0.5+t)S$
5	A/E	0.0	0.0	$-S$
6	B	$+k$	$+\ell_1$	$-(1+t)S$
7	C	0.0	$+\ell_2$	$-1.5S$
8	D	$-k$	$+\ell_3$	$-(1.5+t)S$
9	A/E	0.0	0.0	$-2S$
10	B	$+k$	$+\ell_1$	$-(2+t)S$
11	C	0.0	$+\ell_2$	$-2.5S$
12	D	$-k$	$+\ell_3$	$-(2.5+t)S$
13	A/E	0.0	0.0	$-3S$

The S_4 symmetry of **1** (space group $I\bar{4}$; asymmetric unit depicted in Fig. S1↔) simplifies matters significantly since $r_{AB} = r_{CD}$, $r_{BC} = r_{DE}$ and $z_C = z_E/2$. The latter relationship allows for the rational *z*-direction translation shown in Fig. 2c where the dimensionless constant *t* is responsible for scaling the step size *S* over the five atoms making up one turn. The O_1-Zn_2 interatomic separation is given by

$$r_{AB} = \sqrt{(x_B - x_A)^2 + (y_B - y_A)^2 + (z_B - z_A)^2}$$

where the Cartesian coordinates refer to those in the model derived from the geometry-optimized 100 K crystal structure. The square of the r_{AB} bond length for the incremented *c* axis stepped from its 100 K value by a quantity *S*, $c' = c + S$, is expressed as

$$r'^{2}_{AB} = r^2_{AB} + k^2 + 2k(x_B - x_A) + \ell_1^2 + 2\ell_1(y_B - y_A) + t^2S^2 - 2tS(z_B - z_A)$$

where *k* and ℓ_1 are the stepping variables in the *x* and *y* directions, respectively, for *B*-group atoms. By assuming that the O_1-Zn_2 coordination bond length remains constant, that is, $r'_{AB} = r_{AB}$, the preceding expression is simplified to

$$k^2 + 2k(x_B - x_A) + \ell_1^2 + 2\ell_1(y_B - y_A) + t^2S^2 - 2tS(z_B - z_A) = 0$$

This assumption is validated by the theoretical investigations of anomalous thermal expansion discussed in the introduction. In MD simulations of MOF-5 Han *et al.*[10] found negligible change in Zn-O coordination bond lengths, while Goodwin and co-workers[13,15,16] ascribed anisotropic thermal expansion in $Ag_3[Co(CN)_6]$ to the rigidity of the Co-CN-Ag-NC-Co linkages.

Applying the same reasoning to the bond length for Zn_2-O_3, r_{BC}, the following is found:

$$k^2 - 2k(x_C - x_B) + \ell_3^2 + 2\ell_3(y_C - y_B) + (0.5 - t)S[(0.5 - t)S - 2(z_C - z_B)] = 0$$

where ℓ_3 is the variable controlling the translation in the *y* direction for the *D*-group atoms. The translation of the *C*-group atoms in the *y* direction is controlled by the variable $\ell_2 = \ell_1 + \ell_3$. The value of constant *t* can be obtained by substituting for the values of the parameters that would render the coordination helix fully stretched out on the *z* axis. This is the case when $c' = 2r_{AB} + 2r_{BC}$ (see Table S1↔) and yields $t = 0.0995$. By equating the two preceding equations (and inducing cancellation of terms due to the reorientation of the model) an expression in terms of variables in the *y* and *z* directions only is obtained:

$$(1 - Y^2)\ell_1^2 + 2\ell_1[(y_B - y_A) - Y(y_C - y_B)] - 2tS(z_C - z_A) + S(z_C - z_B) - (0.25 - t)S^2 = 0$$

where it is recognised that $\ell_3 = Y\ell_1$ with constant $Y = y_D/y_B = 10.085$. By solving this expression quadratically, an expression for ℓ_1 in terms of *S* is obtained from which a quadratic expression for *k* also as a function of *S* follows directly. All the variables and, thereby, the movement of all atoms in the coordination helix (*cf.* Table 2) are therefore quantified by the value of variable *S* alone.

A direct comparison to the experimental thermal expansion results can be made by considering how the model predicts variation in the unit cell parameters. Since there are four ···Zn-O(H)-Zn-O(H)··· coordination helices present in a unit cell of **1** the simultaneous change in unit cell length with $\Delta c = S$ is then $\Delta a = \Delta b = -2k + \ell_2$ (recall from Fig. 2b that $k > 0$ and $\ell_n < 0$). In Fig. 3a it can be seen that the model underestimates the decrease in the *a* (equal to *b*) unit cell parameter with respect to the *c* parameter. This results in an overestimation of the volumetric PTE (Fig. 3b).

The truncated ligand moieties are furthermore assumed to remain rigid (in the geometries found in the 100 K structure obtained by SCD, although hydrogen atom positions along with the disordered benzoate of the ligand were optimized using periodic DFT) and are translated along with the zinc atoms to which they coordinate. This allows for the imidazole and benzoate groups to simply be translated as a single *B*- or *D*-group entity (Table 2). A consequence of this assumption is that the N-Zn-O_{carb} valence angle is maintained at its value in the 100 K crystal structure during simulations (Fig. 3c). This is in contrast to the SCD structural data (Table 1) where this angle increases slightly with temperature (by Ψ1.5% between 100 and 370 K). A depiction of the coordination helix of the mechanistic model for an exaggerated value of the stepping variable in the *z*-dimension, namely $S = 1.0$ Å, is shown in

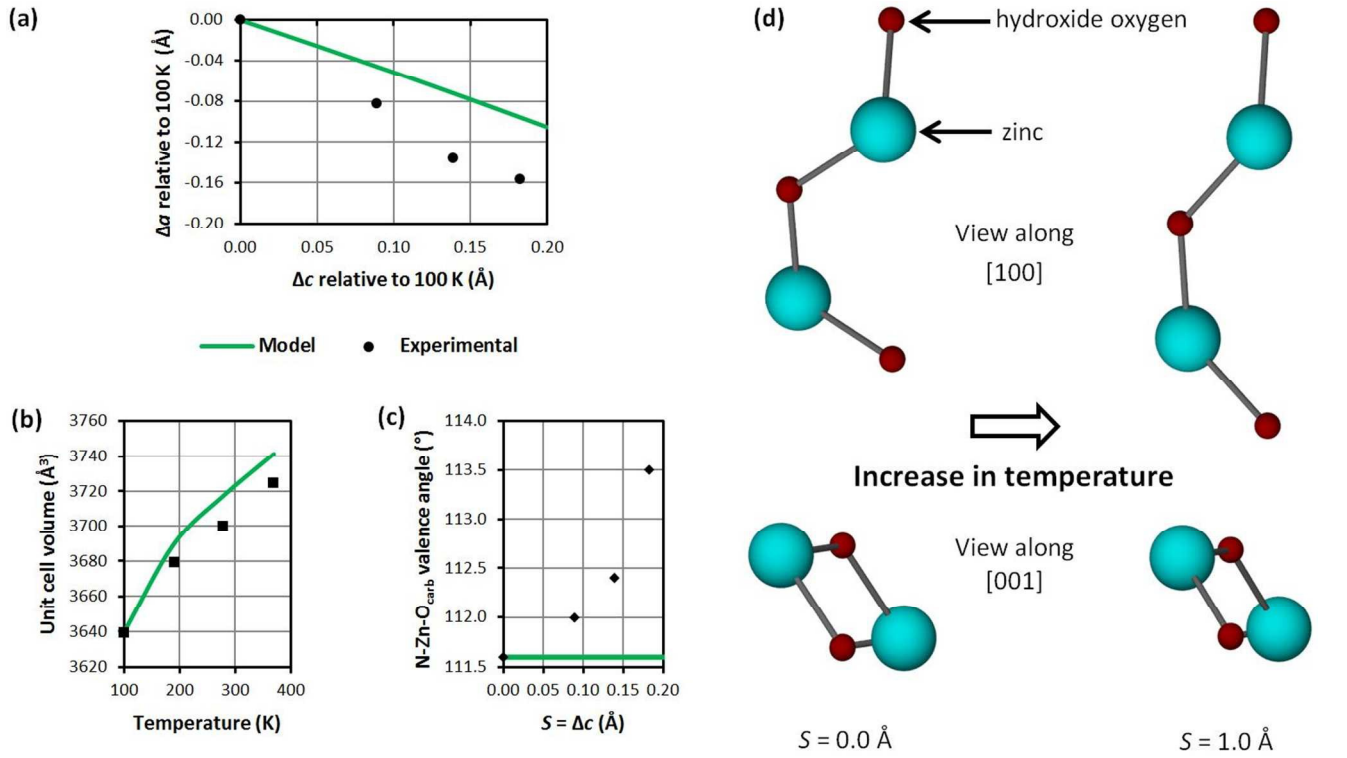

Fig. 3d to illustrate the convergent expansion mechanism along the *c* axis.

Fig. 3 (a) Comparison of the change in unit cell parameters of **1** as obtained from variable temperature SCD structure determinations[12] to those predicted by the mechanistic model (relative to the 100 K structure, or *S* = 0.0 Å model). A comparison of variation in unit cell volume is made in (b), while (c) shows the invariance of the N-Zn-O_{carb} valence angle of the model in contrast to the SCD structural data (*cf.* Table 1). (d) Schematic representation of the modelled temperature dependent convergent expansion mechanism of the coordination helix of **1** showing elongation in the *c* direction and contraction in the *ab* plane.

Molecular dynamics (MD) simulations

To investigate the temperature dependence of the unit cell parameters in **1**, MD simulations were carried out in the isothermal-isobaric, or NPT, ensemble using the program Forcite accessed *via* the Materials Studio suite.[17] The Parrinello-Rahman barostat was used since it allows for change of both unit cell shape and volume during a simulation under constant external pressure.[18] This is essential for attempting to reproduce the experimentally observed *anisotropic* thermal expansion of **1**. The Berendsen thermostat[19] was found to best regulate temperature for the system under investigation.

Simulations were carried out in the temperature range 0 to 400 K in 25 K increments starting with the Molecular Mechanics geometry-optimized 100 K crystal structure of **1**. The general purpose DREIDING force field[20] yielded the best results if used in conjunction with the *charge equilibration* scheme (QEq)[21] and Ewald summation for nonbonded interactions. Simulations were carried out for 200 ps with 1 fs steps, with average values for internal coordinates involving zinc and unit cell lengths taken from the last 100 ps.

Density Functional Theory (DFT) calculations

Calculations of the molecular mechanistic model were carried out *in vacuo* at 0 K using the Gaussian 09 software package (Revision D.01).[22] The B3LYP,[23] M06,[24] PBEPBE[25] and ωB97XD[26] density functionals were used in conjunction with the 6-31G,[27] cc-PVDZ[28] and TZVP[29] basis sets. The local nature of standard density functionals prevents their accurate modelling of dispersion interactions. The B3LYP and M06 functionals were therefore augmented with the second (GD2)[30] and third (GD3)[31] generation of the dispersion correction scheme of Grimme and co-workers, respectively. In order to impose a degree of symmetry and to minimize the number of free variables, all hydrogen atoms were specified in terms of the unique internal coordinates of the asymmetric unit. Reported energies refer to electronic energies after addition of dispersion corrected nuclear repulsion, while zero-point vibrational and thermal energy corrections were neglected.

Periodic DFT calculations

Theoretical evaluations of periodic structures were carried out with the DMol^3 module[32] of the Materials Studio program suite. The positions of atoms in the crystal structures of **1** were optimized employing PBEPBE augmented by GD2 with the DNP basis set. (For details see ESI↞.) Calculations were carried out with effective core potential approximations and thermal smearing was applied to expedite SCF convergence.

To speed up calculations, full geometry optimizations (with fixed unit cell parameters) were carried out on the primitive cell, that is, for the tetragonal crystal system, half the conventional unit cell. Single-point energy calculations were subsequently carried out with the same quality settings after the conventional unit cell (space group $I\bar{4}$) was redefined to

confirm that the potential energy is indeed halved for the primitive cell.

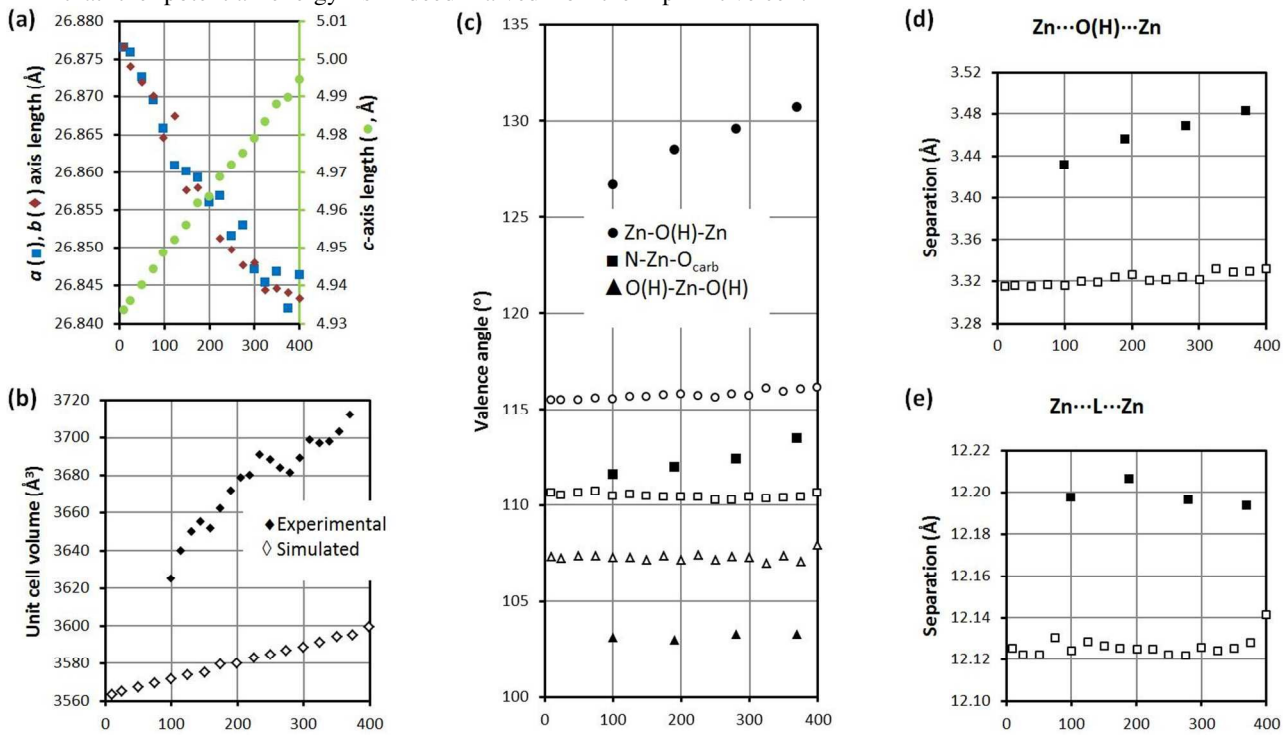

Fig. 4 Unit cell (a) dimensions and (b) volumes of **1** calculated in the NPT ensemble employing the DREIDING force field and the QEq charge scheme. The abscissas of each plot shows variation in temperature (in Kelvin). In (b) the experimental volume change is plotted from SCD data of Fig. 1b while in (c) a comparison is made between experimental (filled symbols) and simulated (open symbols) valence angles involving zinc atoms. Nonbonded Zn···Zn distances across hydroxide groups in the coordination helix and across bridging ligands are compared in (d) and (e), respectively.

Results and discussion

Molecular dynamics (MD) simulations of 1

Results obtained for simulations on one unit cell of **1** are shown in Fig. 4. The observed anisotropic thermal expansion trend (*cf.* Fig. 1b for variable temperature SCD unit cell parameters) is reproduced, but with the simulated change in unit cell volume, $\Delta V_{sim} \approx 24$ Å^3, a factor 4 times smaller than the experimental change in the 100 to 370 K temperature range, $\Delta V_{exp} \approx 88$ Å^3. This is reflected in similarly reduced simulated unit cell length changes (Fig. 4a). It is likely that the origin of the failure of MD to adequately model the magnitude of the volumetric PTE is due to the fact that DREIDING is a generic force field, which may not describe the coordination geometry around the Zn centres with sufficient accuracy. From Fig. 4c it can be seen that the N-Zn-O$_{carb}$ valence angle is underestimated in the simulations, while the O(H)-Zn-O(H) angle is overestimated. DREIDING furthermore utilises a harmonic potential for angle bending with a force constant of 100 kcal mol rad^{-2}, irrespective of the atoms involved. This is highlighted in Fig. 4c, which shows that the computed average Zn-O(H)-Zn angle is underestimated and remains constant over the temperature range considered, as opposed to a steady increase observed for the experimental values. Another consequence of the large angle-bend force constant is that the Zn···O(H)···Zn separation is underestimated and predicted to remain rigid in contrast to the experimentally observed increasing trend, as shown in Fig. 4d. This is expected to be a major contributor to the large deviation in the predicted unit cell volume change in that the length of the crystallographic *c* axis (along which the coordination helix propagates) is not increasing to a large enough extent with increasing temperature. The Zn···L···Zn separation is, however, accurately estimated to within 0.08 Å and remains nearly constant over the temperature range of the simulations (Fig. 4e). This is in line with the SCD structural results reported in Table 1.

Mechanistic model for anisotropic thermal expansion in 1

A rigid-bond model that can be stretched out by varying a single variable to reproduce the expansion of the coordination helix of **1** was introduced in the methods section. DFT results obtained for this mechanistic model are compared here to periodic DFT calculations on the 100, 190, 280 and 370 K SCD structures of **1**. The increased thermal motion of the benzoate moiety decreased the quality of the X-ray data at higher temperatures, with hydrogen atoms poorly positioned or even absent. It was therefore decided to generate the higher temperature structures by imposing their unit cell parameters on the 100 K structure with the same fractional coordinates (including hydrogen atom and benzoate ligand positions that had been previously optimized), and optimizing using periodic DFT. Potential energies relative to the 100 K structure are shown in Fig. 5 indicating a nearly linear rise in the energy as the temperature is increased.

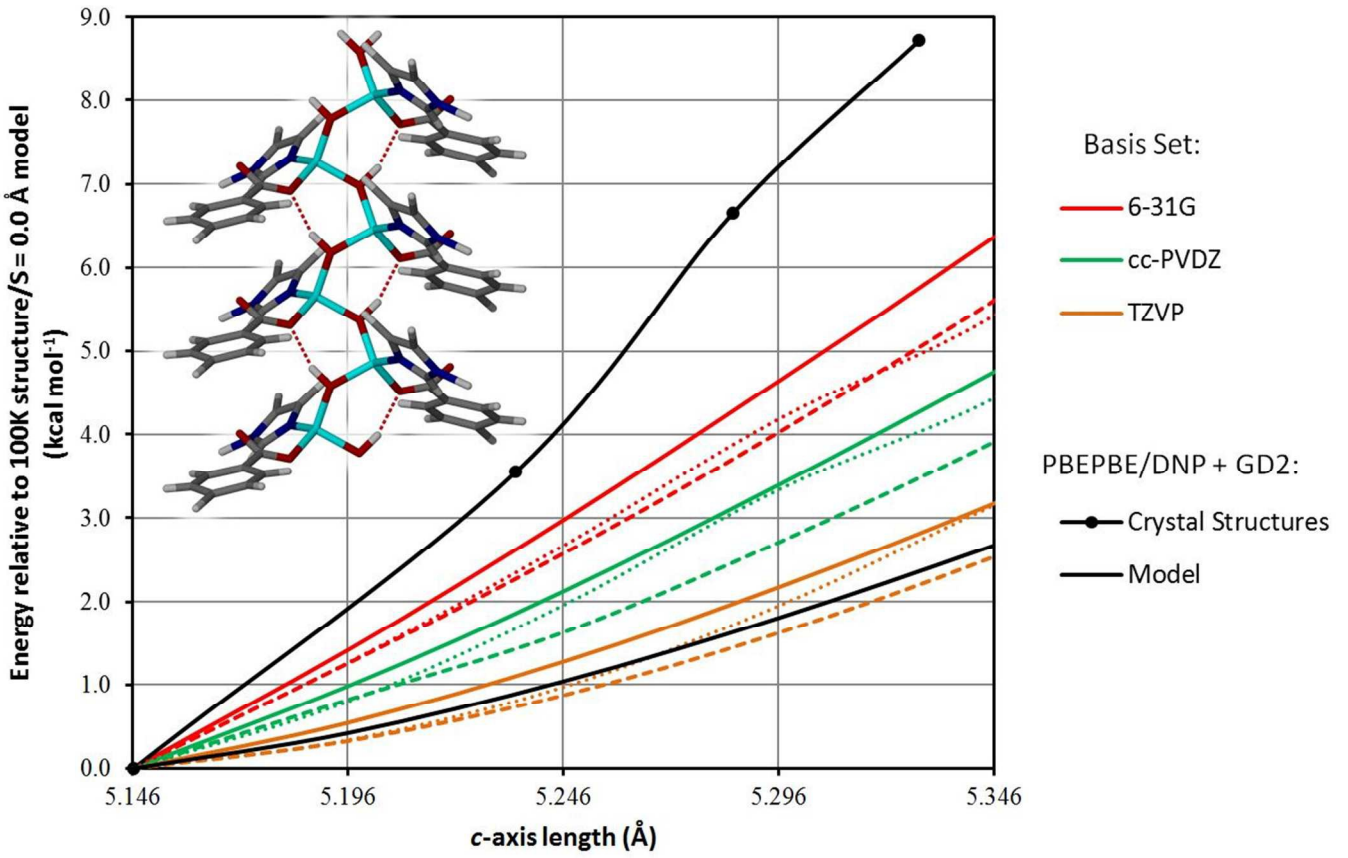

Fig. 5 Comparison of single point energy values for one unit cell of **1** (●) and the scaled results obtained for hydroxide (and water) hydrogen atom geometry optimizations of the mechanistic model (inset) using B3LYP + GD2 (—, coloured), ωB97XD (---) and M06 + GD3 (···) in conjunction with various basis sets. The abscissa shows the effective *c*-axis length calculated as $c' = c + S$. Also shown is the potential energy profile obtained for the model (—) at the same level of theory as the periodic DFT single-point energy calculations.

A model of the representation shown in Fig. 2a was obtained from the optimized 100 K structure and the variable *S* was stepped between 0.00 and 0.20 Å in 0.05 Å increments to yield a *c'* range of 5.146 to 5.346 Å, which corresponds to the experimental *c*-axis length variation in the temperature range 100 to 370 K (*cf.* Table 1).[12] Hydroxide (and water) hydrogen atom positions of procured models were optimized for each value of *S* at different levels of theory. Energies of the models, scaled by a factor 4/3 to allow comparison to the unit cell single-point energy values (8 zinc atoms per unit cell of **1** *vs.* 6 in the mechanistic model), are shown in Fig. 5 relative to the energy of the $S = 0.0$ Å model.

Also depicted as a solid line in Fig. 5 is the potential energy profile for the model determined using DMol[3] with the same settings as for the periodic single-point energy calculations. The magnitude of the results for the TZVP Gaussian-type orbital (GTO) basis set matches the numerical DNP basis set results, with the ωB97XD (dashed lines) potential energy profile closely resembling that obtained with the PBEPBE functional implemented in DMol[3]. Additional comparisons for different basis sets are made in Figs. S8-S10 of the ESI†. The DFT energy of the model increases steadily as the coordination helix lengthens, although the effect is underestimated in comparison to the periodic DFT results. This corresponds to improper modelling of the distortion of the coordination geometry of zinc, as was highlighted in Fig. 3. In addition, truncation of the ligand for computational simplification leads to a mistreatment of the steric repulsion between neighbouring turns on the coordination helix, while replacement of a hydroxide ion by a water molecule produces incorrect stereo-electronic effects. Nevertheless, despite the gross assumptions made in developing the model, notwithstanding the absence of cooperative crystal field effects, the correlation between the crystallographic and the scaled model energies is remarkable. These results confirm that a concerted change in the coordination sphere of the zinc centre so as to elongate the coordination helix in the *c* direction (Zn-O(H)-Zn angles enlarge), while pulling the largely unaltered rigid ligands closer together in the *ab* plane (Zn···L···Zn distance constant) is the dominating causative factor for the observed anisotropic thermal expansion of **1**.

Conclusions

Anomalous thermal expansion of a three-dimensional MOF was investigated by theoretical means. Initially, it was found that Molecular Dynamic simulations in the NPT ensemble employing the DREIDING force field and QEq charges could successfully reproduce the observed trends in the unit cell parameters of **1**. Computed values were, however, found to be

generally underestimated owing to shortcomings of the DREIDING force field. A rigid-bond mechanistic model was developed that is capable of reproducing the observed convergent elongation of the zinc-hydroxide-zinc coordination helix along the crystallographic *c*-axis. The model comprises six zinc centres with ligands truncated to imidazole and benzoate moieties, while a terminating hydroxide was converted into a coordinating water molecule for charge neutrality. The three-dimensional movement of all atoms of the coordination helix of the mechanistic model is controlled by a single variable, namely *S*, while truncated ligand moieties are moved as the zinc atoms they are coordinated to become displaced upon changing the value of *S*. The stepping variable *S* is defined to elongate the coordination helix from its 100 K SCD value to a new value $c' = c + S$. In order to correspond to the experimental 100 to 370 K *c*-axis length range of 5.146-5.3287 Å, *S* was stepped from 0.00 to 0.20 Å in 0.05 Å increments.

Previously obtained 100, 190, 280 and 370 K crystal structures of **1** were evaluated by periodic DFT. The nearly linear rise in potential energy determined for higher temperature structures is successfully reproduced by the mechanistic model as stepping variable *S* is incremented. From this favourable comparison it can be concluded that a concerted change in the coordination geometry of the zinc centre so as to elongate the coordination helix in the *c* direction, while simultaneously pulling the linking ligands closer together in the *ab* plane, is the dominating causative factor contributing to the anomalous thermal expansion of MOF **1**. Development and application of similar mechanistic models to reproduce energy changes observed for other compounds that exhibit anomalous physical properties will be undertaken in the future.

Acknowledgements

LJB and CE thank the National Research Foundation (NRF) of South Africa and Stellenbosch University for financial support. We also thank the Centre for High Performance Computing (CHPC) in Cape Town for the use of their resources.

References

1 G. D. Barrera, J. A. O. Bruno, T. H. K. Barron and N. L. Allan, *J. Phys. Condens. Matter*, 2005, **17**, R217.
2 I. D. Brown, *Acta Crystallogr.*, 1992, **B48**, 553; I. D. Brown, A. Dabkowski and A. McCleary, *Acta Crystallogr.*, 1997, **B53**, 750.
3 W. Miller, C. W. Smith, D. S. Mackenzie and K. E. Evans, *J. Mater. Sci.*, 2009, **44**, 5441.
4 K. Takenaka and H. Takagi, *Appl. Phys. Lett.*, 2005, **87**, 261902.
5 J. L. Korčok, M. J. Katz and D. B. Leznoff, *J. Am. Chem. Soc.*, 2009, **131**, 4866.
6 A. W. Sleight, *Endeavour*, 1995, **19**, 64; T. A. Mary, J. S. O. Evans, T. Vogt and A. W. Sleight, *Science*, 1996, **272**, 90.
7 H. Li, M. Eddaoudi, M. O'Keeffe and M. Yaghi, *Nature*, 1999, **402**, 276.
8 J. L. C. Rowsell, E. C. Spencer, J. Eckert, J. A. K. Howard and O. M. Yaghi, *Science*, 2005, **309**, 1350.
9 D. Dubbeldam, K. S. Walton, D. E. Ellis and R. Q. Snurr, *Angew. Chem. Int. Ed.*, 2007, **46**, 4496.
10 S. S. Han and W. A. Goddard, III, *J. Phys. Chem. C*, 2007, **111**, 15185.
11 N. Lock, Y. Wu, M. Christensen, L. J. Cameron, V. K. Peterson, A. J. Bridgeman, C. J. Kepert and B. B. Iversen, *J. Phys. Chem. C*, 2010, **114**, 16181; N. Lock, M. Christensen, Y. Wu, V. K. Peterson, M. K. Thomsen, R. O. Piltz, A. J. Ramirez-Cuesta, G. J. McIntyre, K. Noren, R. Kutteh, C. J. Kepert, G. J. Kearley and B. B. Iversen, *Dalton Trans.*, 2013, **42**, 1996.
12 I. Grobler, V. J. Smith, P. M. Bhatt, S. A. Herbert and L. J. Barbour, *J. Am. Chem. Soc.*, 2013, **135**, 6411.
13 A. L. Goodwin, M. Calleja, M. J. Conterio, M. T. Dove, J. S. O. Evans, D. A. Keen, L. Peters and M. G. Tucker, *Science*, 2008, **319**, 794.
14 L. Pauling and P. Pauling, *Proc. Natl. Acad. Sci. U. S. A.*, 1968, **60**, 362.
15 M. Calleja, A. L. Goodwin and M. T. Dove, *J. Phys. Condens. Matter*, 2008, **20**, 255226.
16 M. J. Conterio, A. L. Goodwin, M. G. Tucker, D. A. Keen, M. T. Dove, L. Peters and J. S. O. Evans, *J. Phys. Condens. Matter*, 2008, **20**, 255225.
17 *Materials Studio*, Release 7.0, Accelrys Software Inc., San Diego, USA, 2011.
18 G. J. Martyna, D. J. Tobias and M. L. Klein, *J. Chem. Phys.*, 1994, **101**, 4177.
19 H. J. C. Berendsen, J. P. M. Postma, W. F. Van Gunsteren, A. DiNola and J. R. Haak, *J. Chem. Phys.*, 1984, **81**, 3684.
20 S. L. Mayo, B. D. Olafson and W. A. Goddard, III, *J. Phys. Chem.*, 1990, **94**, 8897.
21 A. K. Rappé and W. A. Goddard III, *J. Phys. Chem.*, 1991, **95**, 3358.
22 M. J. Frisch, G. W. Trucks, H. B. Schlegel, G. E. Scuseria, M. A. Robb, J. R. Cheeseman, G. Scalmani, V. Barone, B. Mennucci, G. A. Petersson, H. Nakatsuji, M. Caricato, X. Li, H. P. Hratchian, A. F. Izmaylov, J. Bloino, G. Zheng, J. L. Sonnenberg, M. Hada, M. Ehara, K. Toyota, R. Fukuda, J. Hasegawa, M. Ishida, T. Nakajima, Y. Honda, O. Kitao, H. Nakai, T. Vreven, J. A. Montgomery Jr., J. E. Peralta, F. Ogliaro, M. Bearpark, J. J. Heyd, E. Brothers, K. N. Kudin, V. N. Staroverov, T. Keith, R. Kobayashi, J. Normand, K. Raghavachari, A. Rendell, J. C. Burant, S. S. Iyengar, J. Tomasi, M. Cossi, N. Rega, J. M. Millam, M. Klene, J. E. Knox, J. B. Cross, V. Bakken, C. Adamo, J. Jaramillo, R. Gomperts, R. E. Stratmann, O. Yazyev, A. J. Austin, R. Cammi, C. Pomelli, J. W. Ochterski, R. L. Martin, K. Morokuma, V. G. Zakrzewski, G. A. Voth, P. Salvador, J. J. Dannenberg, S. Dapprich, A. D. Daniels, O. Farkas, J. B. Foresman, J. V. Ortiz, J. Cioslowski and D. J. Fox, *GAUSSIAN 09*, Revision D.01, Gaussian, Inc., Wallingford CT, 2013.
23 A. D. Becke, *Phys. Rev. A*, 1988, **38**, 3098; C. Lee, W. Yang and R. G. Parr, *Phys. Rev. B*, 1988, **37**, 785; B. Miehlich, A. Savin, H. Stoll and H. Preuss, *Chem. Phys. Lett.*, 1989, **157**, 200; A. D. Becke, *J. Chem. Phys.*, 1993, **98**, 5648; P. J. Stephens, F. J. Devlin, C. F. Chabalowski and M. J. Frisch, *J. Phys. Chem.*, 1994, **98**, 11623.
24 Y. Zhao and D. G. Truhlar, *Theor. Chem. Acc.*, 2008, **120**, 215.

25 J. P. Perdew, K. Burke and M. Ernzerhof, *Phys. Rev. Lett.*, 1997, **78**, 1396; J. P. Perdew, K. Burke and M. Ernzerhof, *Phys. Rev. Lett.*, 1996, **77**, 3865.
26 J.-D. Chai and M. Head-Gordon, *Phys. Chem. Chem. Phys.*, 2008, **10**, 6615.
27 W. J. Hehre, R. Ditchfield and J. A. Pople, *J. Chem. Phys.*, 1972, **56**, 2257; P. C. Hariharan and J. A. Pople, *Theor. Chim. Acta*, 1973, **28**, 213.
28 T. H. Dunning, Jr., *J. Chem. Phys.*, 1989, **90**, 1007; R. A. Kendall, T. H. Dunning, Jr. and R. J. Harrison, *J. Chem. Phys.*, 1992, **96**, 6796; D. E. Woon and T. H. Dunning, Jr., *J. Chem. Phys.*, 1993, **98**, 1358; K. A. Peterson, D. E. Woon and T. H. Dunning, Jr., *J. Chem. Phys.*, 1994, **100**, 7410; A. K. Wilson, T. van Mourik and T. H. Dunning, Jr., *J. Mol. Struct. THEOCHEM*, 1996, **388**, 339.
29 A. Schäfer, H. Horn and R. Ahlrichs, *J. Chem. Phys.*, 1992, **97**, 2571; A. Schäfer, C. Huber and R. Ahlrichs, *J. Chem. Phys.*, 1994, **100**, 5829.
30 S. Grimme, *J. Comput. Chem.*, 2006, **27**, 1787.
31 S. Grimme, J. Antony, S. Ehrlich and H. Krieg, *J. Chem. Phys.*, 2010, **132**, 154104.
32 B. Delley, *J. Chem. Phys.*, 1990, **92**, 508; B. Delley, *J. Chem. Phys.*, 2000, **113**, 7756.

A mechanistic model is developed to reproduce concerted changes in the internal coordinates of the coordination helix of a MOF and evaluated using DFT.